



**HAL**  
open science

## **Cirrus crystal fall velocity estimates using the Match method with ground-based lidars: first investigation through a case study**

Davide Dionisi, Philippe Keckhut, Christophe Hoareau, Nadège Montoux, F. Congeduti

► **To cite this version:**

Davide Dionisi, Philippe Keckhut, Christophe Hoareau, Nadège Montoux, F. Congeduti. Cirrus crystal fall velocity estimates using the Match method with ground-based lidars: first investigation through a case study. *Atmospheric Measurement Techniques*, 2013, 6 (2), pp.457-470. 10.5194/amt-6-457-2013 . hal-00724297

**HAL Id: hal-00724297**

**<https://hal.science/hal-00724297>**

Submitted on 26 Dec 2014

**HAL** is a multi-disciplinary open access archive for the deposit and dissemination of scientific research documents, whether they are published or not. The documents may come from teaching and research institutions in France or abroad, or from public or private research centers.

L'archive ouverte pluridisciplinaire **HAL**, est destinée au dépôt et à la diffusion de documents scientifiques de niveau recherche, publiés ou non, émanant des établissements d'enseignement et de recherche français ou étrangers, des laboratoires publics ou privés.



# Cirrus crystal fall velocity estimates using the Match method with ground-based lidars: first investigation through a case study

D. Dionisi<sup>1,2</sup>, P. Keckhut<sup>1</sup>, C. Hoareau<sup>3</sup>, N. Montoux<sup>4</sup>, and F. Congeduti<sup>2</sup>

<sup>1</sup>Laboratoire Atmospheres, Milieux, Observations Spatiales-IPSL, UMR8190, CNRS/INSU, UVSQ-UPMC, UniverSud Paris, Guyancourt, France

<sup>2</sup>Istituto di Scienze dell' Atmosfera e del Clima, Consiglio Nazionale delle Ricerche, Roma, Italy

<sup>3</sup>LMD, UMR8539, INSU-CNRS, UPMC, Ecole Polytechnique, 91128, Palaiseau Cedex, France

<sup>4</sup>Laboratoire de Meteorologie Physique, Blaise Pascal University, Aubiere, France

Correspondence to: D. Dionisi (davide.dionisi@latmos.ipsl.fr)

Received: 18 May 2012 – Published in Atmos. Meas. Tech. Discuss.: 20 August 2012

Revised: 14 January 2013 – Accepted: 28 January 2013 – Published: 22 February 2013

**Abstract.** Cirrus ice particle sedimentation velocity ( $v_s$ ) is one of the critical variables for the parameterization of cirrus properties in a global climate model (GCM). In this study a methodology to estimate cirrus properties, such as crystal mean fall speed, through successive lidar measurements is evaluated. This “Match” technique has been applied on cirrus cloud observations and then tested with measurements from two ground-based lidars located in the Mediterranean area. These systems, with similar instrumental characteristics, are installed at the Observatory of Haute Provence (OHP, 43.9° N, 5.7° E) in France and at Rome Tor Vergata (RTV, 41.8° N, 12.6° E) in Italy. At a distance of approximately 600 km, the two lidar stations have provided systematic measurements for several years and are along a typical direction of an air path. A test case of an upper tropospheric cirrus, observed over both sites during the night between 13 and 14 March 2008, has been selected and the feasibility of the Match-cirrus approach investigated through this case. The analysis through lidar principal parameters (vertical location, geometrical thickness and optical depth) reveals a case of a thin sub-visible cirrus (SVC) located around the tropopause. A first range of values for  $v_s$  (1.4–1.9 cm s<sup>-1</sup>, consistent with simple-shaped small crystals) has been retrieved with a simplified approach (adiabatic transport and “frozen” microphysical conditions inside the cirrus). The backward trajectory analysis suggests a type of cirrus formed by large-scale transport processes (adiabatic cooling of moist air masses coming from the subtropical area around Mexico gulf), which is characterized by a long atmospheric lifetime

and horizontal extension of several hundred km. The analysis of this case study reveals that many uncertainties reduce the confidence of the retrieved estimates of the crystal fall velocity. However, this paper allows for assessing the technique feasibility by identifying the main critical issues for future similar investigations.

This study shows that such approach is feasible; however, the methodology should be improved and some directions have been suggested for future campaigns.

## 1 Introduction

Sedimentation of ice crystal is an important process in clouds and has a large influence on their microphysical properties. In situ measurements (Heymsfield and Miloshevich, 2003) have shown that the top of a cirrus cloud is mainly composed of small but numerous ice crystals, whereas the bottom consists more of few large crystals. Such vertical distributions can have some local cooling or warming radiative effects (Khvorostyanov and Sassen, 2002). In a study that related climate sensitivity to atmospheric global climate model (GCM) parameters, Sanderson et al. (2008) identified the ice crystal fall speed as the second most influential parameter to climate sensitivity, and a decrease in fall speed was related to an increase in cirrus cloud coverage, humidity and long-wave cloud forcing. Similar conclusions have been obtained using Lagrangian numerical simulations (Montoux et al., 2010). It has been also demonstrated (Jakob, 2002) that, in the weather

forecast model of the European Centre for Medium Range Weather Forecast (ECMWF), the global mean integral radiation flux divergence decreases from  $110 \text{ W m}^{-2}$  to  $90 \text{ W m}^{-2}$  for assumed fixed values of the crystal fall speed from  $0.1$  to  $2 \text{ m s}^{-1}$ . The importance of a correct representation of the sedimentation in large-scale models appears clearly when comparing the difference of  $20 \text{ W m}^{-2}$  with the  $3.5 \text{ W m}^{-2}$  radiative forcing due to the greenhouse effect for doubling  $\text{CO}_2$ . Sedimentation is also important in the evolution of the cloud structure and in the humidity field inside the cirrus as sedimenting ice crystals can quench in-cloud nucleation (Spichtinger and Gierens, 2009).

One of the main missing pieces of information for the determination of cirrus impacts was, up until recently, the altitude characterization of their vertical location and stratification. Cirrus clouds that consist of a small number of particles exhibit large scattering but tenuous optical depth. Spaceborne passive remote sensing instruments in the infrared, due to their low sensitivity, are not able to vertically characterize a part of these clouds, as in cases of a semitransparent cirrus (high, thin cirrus) and multi-layer clouds (thin cirrus overlying low clouds) (Stubenrauch et al., 1999). On the contrary, active remote sensing methods based on lidar can detect high and thin cirrus clouds with high vertical spatial and temporal resolution. Lidar measurements give access to backscattering vertical profiles of cirrus clouds, from which it is possible to directly derive their absolute geometric height and thickness with typical resolutions of 10 to 100 m (Sassen et al., 2008). Backscattering ratio, which is related to the number of particles, their size, shape, composition and phase, can provide, with some assumptions, information about these quantities. Lidar can be operated continuously, which then gives some indication of the variability of the cirrus above the instrument. For ground-based measurements, this variability is mainly related to advection and to the cirrus life cycle, as cirrus particles are both transported by the mean flow and subjected to ice crystal formation processes. Several statistics have been derived from these measurements (Goldfarb et al., 2001; Sassen and Campbell, 2001; Cadet et al., 2005), but the global coverage of these observations, although they can provide useful information about the occurrence and cirrus types, is too poor to deduce accurate global radiative estimates. Similar measurements are now available from space with the Calipso mission (Sassen et al., 2009; Taylor et al., 2011) that show good agreement with ground-based stations (Dupont et al., 2010), and provide better knowledge of the horizontal distribution of the ice clouds (Chepfer et al., 2008). However, these measurements do not directly provide information about the life cycle of the cirrus clouds because space-borne passive measurements do not retrieve cloud altitudes accurate enough for such investigations.

Vertical velocity in cirrus clouds can be measured through Doppler radar by averaging Doppler velocity over a long period (Orr and Kropfli, 1999) and by explicitly solving ice crystal velocity within the sample volume using 3 Doppler

moments (Deng and Mace, 2006). The main limitation of the technique is that it is mainly sensitive to large particles (i.e. effective ice crystal radius  $> 50 \mu\text{m}$ ). On the contrary, the application of coherent Doppler lidar, which provides very accurate measurements of vertical velocity also in cirrus nucleating zones (Grund et al., 2001), is limited to optically thin clouds. A methodology which couples radar and lidar measurements has been developed (Tinel et al., 2005), but, as shown by Donovan and van Lammeren (2001), this cloud radar–lidar synergy cannot retrieve ice crystals with an effective radius lower than  $10 \mu\text{m}$ .

However, ice particle growth, sedimentation, aggregation, light absorption, and evaporation could be investigated using a Lagrangian tracking method: The detailed locations and so the history of individual ice particle clusters and physical properties would be tracked as a function of time. This method, known as the Match method (von der Gathen et al., 1995), consists in making a measurement at a given place and time, using forward trajectory to see if the sounded air mass will transit, by chance, over another sites equipped with similar instruments, and making a second measurement of the same air mass at the corresponding time matching with the forecast trajectory.

Observations from different locations within a given region of interest, coupled with Lagrangian trajectories, were developed to quantify chemical ozone loss in the Arctic stratosphere (Rex et al., 1998, 1999) using ozonesondes. They were then applied to water vapour satellite data (Luo and Rossow, 2004), and, more recently, to polar stratospheric cloud (PSC) studies during the International Polar Year (IPY).

The objective of this study was to describe the first observations obtained with two ground-based lidar, investigating existing data archives from both stations in order to assess the feasibility of a possible future observation strategy that couples lidar measurements to a Lagrangian tracking method to study cirrus cloud formation, air mass history and, in particular here, mean cirrus fall speed. The Eulerian characteristics of lidar technique, its typical temporal and vertical resolution in upper troposphere (tens of minutes and of meters), together with cirrus high horizontal variability, do not allow for deriving sedimentation velocity through measurements of only one lidar. In fact, to appreciate the sedimentation speed of cirrus crystals (between  $0.1$ – $200 \text{ cm per second}$  for ice crystals with an effective radius from  $5$  to  $500 \mu\text{m}$ , Schmitt and Heymsfield, 2009) during a single lidar session with a vertical resolution of  $75 \text{ m}$ , lidar measurements should last at least two or three hours and, within this period, cirrus clouds should exhibit a negligible variability in order to explain changes in cirrus mean height only with crystal fall speed.

The proposed observing strategy includes using several lidar systems and a trajectory tracking method in order to measure the same cirrus cloud at different times and then, because of advection, at different places. Exploiting the high

resolution of lidar measurements to characterize cirrus vertical structures and the so-called Match technique, the idea is to apply this methodology to investigate the mean changes of the microphysical cloud properties over quasi-stationary cloud periods (Hoareau et al., 2009) through the analysis of the variations of the derived lidar parameters observed by successive measurements located along the estimated directions of the air mass trajectory. In particular, the vertical shape of the cirrus over few hours of transport can be associated with crystal vertical distribution and, partly, with the sedimentation velocity.

In comparison to a lidar–radar synergy (Tinel et al., 2005), the employment of the Match–lidar observation strategy proposed here, providing unique measurements about the mean changes of the microphysical cloud properties during a cirrus advection over hundreds of km, could extend the investigation also to subvisible (SVC, with ice crystals  $< 10\ \mu\text{m}$ ) and optically thick (with a visible optical depth up to 1.5–2) cirrus. This would bring helpful information for the parameterization of cirrus formation and evolution in GCM. Eventually, in the future, this approach could also be used with a lidar–radar approach.

The advanced lidar systems at Observatory of Haute-Provence (OHP) and at Rome-Tor Vergata (RTV) located, respectively, in the south of France and in central Italy, are at a reciprocal distance of 600 km, along a typical direction of front progression in the Mediterranean area. These geographical favourable conditions and the instrumental characteristics of OHP and RTV lidars (similar in terms of emitted wavelengths and capabilities) suggested testing the Match–lidar cirrus strategy, analysing the existing dataset of these two systems.

Thus, in this work, subsamples of the two lidar have been processed with a common algorithm procedure and coupled with a trajectory analysis. The main idea was to assess the technique feasibility through the study of a Match test. Therefore, a case of upper tropospheric thin cirrus measured over the two sites has been selected and analysed through the Match strategy and the main critical issues of this approach have been characterized.

The paper is organized as follows: in Sect. 2, the main instrumental characteristics of the both lidar systems are briefly described together with the cirrus retrieval algorithms, while Sect. 3 addresses the Match–lidar methodology itself. The results of this approach are provided in Sect. 4, where the developed procedure is applied to both lidar datasets. A test case of an upper tropospheric cirrus observed by the two systems during the night between 13 and 14 March 2008 is studied. The associated uncertainties and the case consistency are discussed. Finally, in Sect. 5, the results, the limitations and the improvements required to quantitatively adopt this technique are discussed as a preparation for the setup of specific campaigns performed on alert.

## 2 Lidar systems description and retrieval of cirrus characteristics

At the OHP (43.9° N, 5.7° E, and 678 m altitude), a program of systematic lidar soundings of stratosphere and troposphere has been running for two decades (Goldfarb et al., 2001). The system utilizes a doubled Nd:YAG laser, which emits a light pulse of  $\sim 10\ \text{ns}$  at 532.2 nm, with 50 Hz repetition rate and 300-mJ average pulse energy. The receiver employs a multiple collecting telescope configuration for NDACC (Network for the Detection of Atmospheric Composition Changes) operations. For the Upper Troposphere/Lower Stratosphere (UTLS) soundings, a single receiving telescope (20 cm diameter) with an adjustable diaphragm to reduce the collector efficiency is used. Transmitted beam and receiver field of view are zenith oriented. The photon counting system has a 0.5 ms bin width, corresponding to an altitude resolution of 75 m; the received backscatter signal is generally averaged over 160 s intervals. The observations are performed at night. The lidar is operated for most of the weather permitting nights, allowing cirrus detection between 100–150 nights per year. The typical time measurement period is 6 h. Raman channels for nitrogen and water vapour were also implemented (Sherlock et al., 1999). Atmospheric temperature measurements are taken from high-resolution (Vaisala RS92) radiosondes launched from Nimes, the closest meteorological station ( $\sim 80\ \text{km}$  east of OHP).

The Rayleigh-Mie-Raman (RMR) lidar located in the suburban area of RTV (41.8° N, 12.6° E, and 107 m altitude), at the Institute of Atmospheric Sciences and Climate (ISAC), utilizes a Nd:YAG laser with second and third harmonic generators which emits two pulsed beams in the green (532.2 nm, 200 mJ energy per pulse) and in the UV (354.8 nm, 400 mJ energy per pulse), with 10 Hz repetition rate and  $\sim 7\ \text{ns}$  pulse width. The green beam is used to receive the elastic backscatter from the air molecules and aerosol particles; the UV beam is used to obtain Raman backscattering signals from water vapour and nitrogen molecules and to calculate the water vapour mixing ratio (Dionisi et al., 2010). Also in this case, a multiple telescope configuration is adopted in the receiver to collect the signal return from different altitude layers and obtain profiles of the interesting parameters over a wide altitude atmospheric interval (Congeduti et al., 1999). The acquisition vertical resolution is 75 m and the signals are integrated over 60 s (600 laser pulses) and recorded. The RMR system is operated in a manual mode and provides 40–60 nighttime measurements per year. High-resolution radiosounding data (Vaisala RS92) are available from the Italian Meteorological Service in Pratica di Mare (25 km south-west of Tor Vergata). These are utilized for the calibration of the water vapour Raman profiles, and to add complementary parameters (e.g. density, temperature, etc.) to the lidar results. Technical characteristics of the two instruments are provided in Table 1.

**Table 1.** Transmitter and receiver characteristics of the OHP and RTV lidar systems.

		Rome-RTV (41.8° N, 12.6° E, 107 m a.s.l)			OHP (43.9° N, 5.7° E, 678 m a.s.l)		
<b>Transmitter</b>							
Laser type	Nd:Yag			Nd:Yag			
Wavelength	532 nm–355 nm			532 nm			
Energy per pulse	200 mJ–400 mJ			400 mJ			
Pulse repetition rate	10 Hz			50 Hz			
beam diameter	45 mm			20 mm			
beam divergence	0.1 mrad			0.4 mrad			
<b>Receiver</b>							
	Collector 1	Collector 2	Collector 3	Collector 1	Collector 2	Collector 3	
Type of telescope	Newtonian array	Newtonian	Newtonian	Newtonian array	Newtonian	Newtonian	
Diameter, f-number	9 · 500 mm, F3	300 mm, F3	150 mm, F3	4 · 500 mm, F3	800 mm, F3	100 mm, F2	
Field of view (mrad)	0.6	0.9	1.8	0.4	0.7	10	
Optic fiber	yes	yes	yes	yes	yes	yes	
<b>Data acquisition</b>							
Raman channels N2	387 nm	387 nm			607 nm		
H <sub>2</sub> O	407 nm	407 nm			660 nm		
Elastic channels	532 nm	532 nm	532 nm	532 nm		532 nm	
Sounding range (km)	2–15 (Raman) 25–80 (elastic)	0.1–5 (Raman) 6–40 (elastic)	0.5–8 (elastic)	25–80 (elastic)	2–10 (Raman)	0.2–30 (elastic)	
Time resolution (sec)	60	60	60	160	160	160	
Vertical resolution (m)	75	75	75	75	75	75	

In cases of Match events (see Sect. 3), the same data analysis procedure is applied to the raw lidar data of the two instruments in order to detect the presence of a cirrus and provide its vertical shape. In particular, this procedure consists in deriving the backscattering ratio (BSR, the ratio between the sum of the Mie and Rayleigh backscattering coefficients and the Rayleigh backscattering coefficient) vertical profiles from the ratio between the return signal at 532 nm and nitrogen Raman signal (Ferrare et al., 2001), and in using this quantity to obtain the optical depth of the mid- and upper-atmosphere (between 7 and 12/13 km, approximately), assuming a fixed value of the lidar ratio (i.e. extinction-to-backscatter ratio, LR, Platt and Diley, 1984), with a temporal resolution of the original raw data.

In order to get a reasonable compromise between measurement accuracy and atmospheric variability, the time series of the optical depth are analysed through an iterative method designed to research discontinuity points in order to define periods of quasi-stationary conditions regarding statistical variability (Lanzante, 1996). Data analyses are then performed on these integrated periods to derive accurate optical cirrus properties (Hoareau et al., 2009). The backscattering profile retrieval is based on the methodology described in Goldfarb et al. (2001) for OHP lidar and slightly modified for the RMR Italian lidar, permitting characterization of cirrus clouds through some lidar principal parameters (LPP) such as the absolute geometric height, thickness, the mean backscattering ratio, the relative height to tropopause and the optical depth.

### 3 Description of the Match cirrus technique

As previously mentioned, the Match method was initially applied to estimate the chemical ozone loss on the Arctic stratosphere and, more recently, to study PSC during IPY. The basic idea of a Match method is as follows: after an air parcel has been probed at a given place and time (departure site), its forward trajectory is calculated; if the air mass transits over (or close to) another site (arrival site) that performs a second sampling with a similar instrument, then the two measurements form a “Match” and can be compared. The comparison of these two successive measurements of the same air mass gives direct information about its composition. A similar approach has been applied here to study cirrus evolution with two ground-based lidar stations, OHP and RTV, which are the departure and the arrival site, respectively. Associated with these lidar measurements, two clusters of five trajectories (backward and forward) are launched for each site at three different altitudes (8, 10 and 12 km, respectively) corresponding to the 3 main cirrus cloud clusters (Keckhut et al., 2006) to find potential Match cases between both sites in the upper troposphere. The central trajectory of each altitude starts at the lidar station and the other four trajectories are started 0.5° each to the north, south, east and west (approximately 55 km in latitude and 40 km in longitude) of the central one. Trajectories are considered reliable (not divergent) only if, at the ending point (i.e. at the arrival lidar station), the sum of the distances between the central and the other four trajectories does not exceed the initial sum of the distances at the starting lidar station of no more than 20 %.

Match cases are those fulfilling two fixed criteria:

- the nearest points to the arrival lidar station of the central trajectory for each of two clusters should be at a distance lower than a maximum value ( $R_{\max}$ , spatial Match condition);
- the time spent by the air mass to move from one site to the other should be included within  $\Delta t_m$ , which is the time lag defined by the lidar measurement starting time of the departure site and the lidar measurement ending time of the arrival site (temporal Match condition).

Uncertainties associated with the Match method are, in general, composed of systematic and random errors. Systematic errors are inherent in the measurement techniques adopted in the Match method (in our case, lidar technique and the trajectory code). Referring to the four sources of random errors attached to the Match method used for ozone loss quantifications, identified by Lehmann et al. (2005), the successive campaigns were helpful in improving the methodology based on the effort of identifying and reducing all the identified sources of error. Similar uncertainties exist when applying the Match method to identifying cirrus properties. The lidar technique itself with one wavelength does not introduce the largest uncertainty while the direct variables are used (altitude and optical depth) and depends on vertical resolution (here 75 m). The cluster trajectory approach, even though used in many applications, represents the largest uncertainties and relies on the accuracy of the meteorological analyses and mainly the vertical wind. The remaining two other error sources, non-zero match radius (i.e. spatial coincidence between the second lidar measurement and the calculated position of the air mass) and deviation between single measurements and mean quantities (i.e. representativeness of individual lidar sessions to describe cirrus mean variations), are two critical points because of the high temporal and spatial variability of cirrus clouds. The contribution of the latter source can be reduced by the quasi-stationary integration approach described previously, which somehow gives an average quantity of the location of the cloud that smooths the local variability due to inhomogeneities of temperature and water vapour fields (Keckhut et al., 2013). A suitable maximum match radius ( $R_{\max}$ ), instead, must be applied to limit the error contribution of the former source. However, the value of  $R_{\max}$  strictly depends on the horizontal extension and variability of the cirrus; for the case considered in this work,  $R_{\max}$  is fixed to 150 km.

If air masses fulfil these conditions and the presence of cirrus is revealed in both lidar datasets, the significant changes of cirrus mean optical characteristics can then be attributed to real changes of the cirrus vertical structures.

## 4 Results

### 4.1 French–Italian experimental setup

The French and the Italian lidar sites are located along one of the typical directions of the front progression in the Mediterranean area. This statement has been confirmed by studying the origin of the air masses arriving daily above the RTV site at 00:00 UTC. In fact, using the GDAS (Global Data Assimilation System) dataset for five years (2006–2010), the 24-h backward trajectories for three different heights (8, 10 and 12 km, respectively) have been calculated through the Hybrid Single-Particle Lagrangian Integrated Trajectory (HYSPPLIT, Draxler and Rolph, 2003) model, in order to determine the frequency of occurrence of the air masses that passed over a  $0.7^\circ \times 0.7^\circ$  grid centred at OHP before arriving at RTV. This analysis has highlighted that the OHP–RTV direction (N–SE) is one of the more frequent directions for the upper tropospheric air mass displacement in the northwest Mediterranean region, and more than 10 % of the air masses, which arrive at RTV at 00:00 UTC, have previously passed over OHP (OHP/RTV air mass coincidence).

Figure 1 depicts the cumulative occurrence (in %) of the time spent by the air masses (at 8, 10 and 12 km; solid, dashed and dotted lines, respectively) to go from OHP to RTV, during the 2006–2010 period. It has to be noted that, for approximately 40 % of the cases (i.e. 4 % of the total number of backward trajectory considered), the time needed to cover the distance between the two sites (approximately 600 km) is lower or equal to 8 h. This value has been fixed as  $\Delta t_m$ . Therefore, during contemporary night-time lidar session, it is possible that the same upper tropospheric air mass has the time to advect from one site to the other one, thus fulfilling the temporal Match condition.

The first requirement consists of finding cirrus cases extending or travelling from OHP to RTV in the dataset of both instruments. For this study, night-time lidar sessions of two-year period 2007–2008 have been considered. The statistics of the number of measurements observed by each lidar and the number of contemporary night-time measurements are resumed in Table 2.

Despite the OHP–RTV upper tropospheric favourite direction, the number of contemporary lidar measurements (and consequently the number of Match sessions) is significantly reduced by the manual-operating mode of the RMR measurement operations. In fact, out of 42 common day lidar sessions, only four cases, in which the upper tropospheric air masses successively passed over OHP and RTV sites, fulfilled the above-stated Match criteria and, in particular, since no coordinated operation was performed at that time, only one case over both sites observed the presence of the same air mass including cirrus clouds. This case refers to the night between 13 and 14 March 2008 where an upper tropospheric thin cirrus has been measured by OHP and RTV lidars.

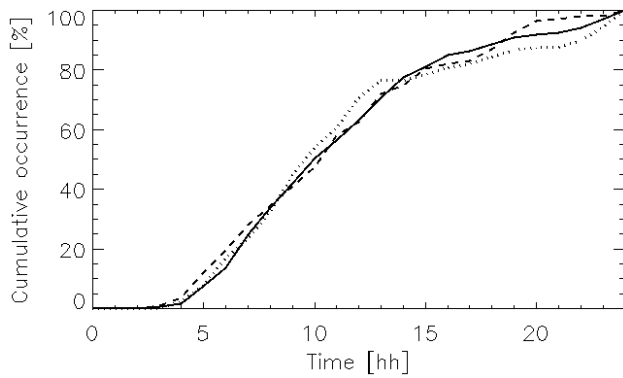


**Fig. 1.** Cumulative occurrence (in %) of the OHP/RTV air mass coincidence in function of the time spent by the air masses (at 8, 10 and 12 km; solid, dashed and dotted lines, respectively) to go from OHP to RTV sites. Backward trajectories have been computed for the 5-yr period (2006–2010).

**Table 2.** Night-time lidar sessions, common days of measurements and Match sessions acquired during the period 2007–2008 by the OHP and RTV lidar systems.

2007–2008	OHP	RTV	Common days	Match sessions
# Lidar sessions	306	71	42	4

#### 4.2 Test case description

Figure 2a and b report the temporal evolution of the BSR measured for this night at OHP and RTV stations, respectively. White vertical lines indicate the quasi-stationary periods identified. According to the procedure described in Sect. 2, the combined use of the elastic and nitrogen Raman channel of the two systems allowed for the characterization of the cirrus observed through lidar principal parameters.

Table 3a and b give the results of this analysis for each quasi-stationary period of the lidar sessions of the two sites. In particular, optical depth  $\tau$  has been estimated independently using both the BSR profile inside the cirrus with a fixed a priori value of LR (particle integration, PI, method, Cadet et al., 2005) and the comparison of the elastic backscattering signals, fitted through the radiosonde density profile, just below and above the cloud (molecular integration, MI, method, Chen et al., 2002). For the cirrus observed through the RTV lidar system, the amount of signal in the nitrogen channel permitted evaluation of  $\tau$  using the extinction of Raman signal below and above the cirrus (Raman method, Ansmann et al., 1992). However, because of the very low optical thickness of the cirrus studied, the optical depths, calculated with MI and the Raman methods, are affected by large errors, as reported by Table 3a and b. The errors associated with optical depths are calculated following the appendix in Chen et al. (2002). Furthermore, it is worth noting that, in

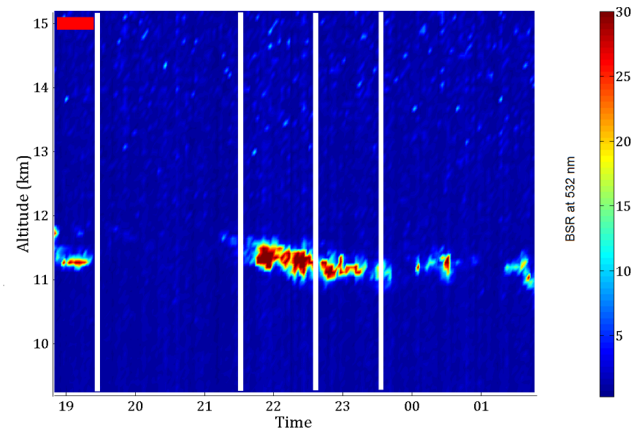


**Fig. 2a.** Contour plot of the backscattering ratio (BSR) calculated from the elastic channel at 532 nm for the lidar session at OHP between 18:48 and 01:44 UTC. White vertical lines identify the quasi-stationary periods. The horizontal red bar indicates the quasi-stationary period used in the Match approach (18:48–19:20 UTC).

cases of optically thin cirrus ( $\tau \ll 1$ , in the visible), the multiple scattering factor has an influence of less than 1 % in the estimation of  $\tau$ ; therefore, no corrections of multiple scattering have been made. The temperature values inside the cirrus for OHP and RTV, as well as the density profiles, are derived from the operational radiosonde launched, respectively, from Nimes (80 km west from the OHP) and Pratica di Mare (25 km south-west from RTV). During the OHP lidar session there is no presence of cirrus between 19:20 and 21:38 UTC, while cirrus is constantly present over the RTV site with a case of two-layer cirrus for the first two hours.

The cirrus clouds sensed through the OHP lidar have similar characteristics of those identified through RMR system. In particular, both cirrus clouds exhibit similar values of optical depth, mean altitude, thickness and intensity of the mean backscattering ratio. These values highlight the presence, over both sites, of a subvisible cirrus (SVC), which has an optical depth always below 0.03 (except for period 2 of the OHP), a thickness varying from 500 m and 1.3 km, an altitude between 10.8 and 11.4 km and a top height that is around the local tropopause (11.24 and 11.10 km for OHP and RTV), which was calculated using radiosonde temperature data and the definition of thermal tropopause.

The 3-D backward trajectories, corresponding to the height of the cirrus envelopes (from 10.7 km to 11.7 km), for the air masses which pass above the OHP site at 19:00 UTC on 13 March 2008 and arrive near RTV site at 01:00 UTC on 14 March 2008 are shown in Fig. 3. For clarity, for each altitude, only central backward trajectories of the reliable clusters are reported. The case considered satisfies both spatial (the air masses pass near the RTV site at about 80 km, within  $R_{\max}$ ) and temporal (the air mass advection time from one site to the other, 6 h approximately, is within  $\Delta t_m$ ) Match conditions (see Sect. 3).

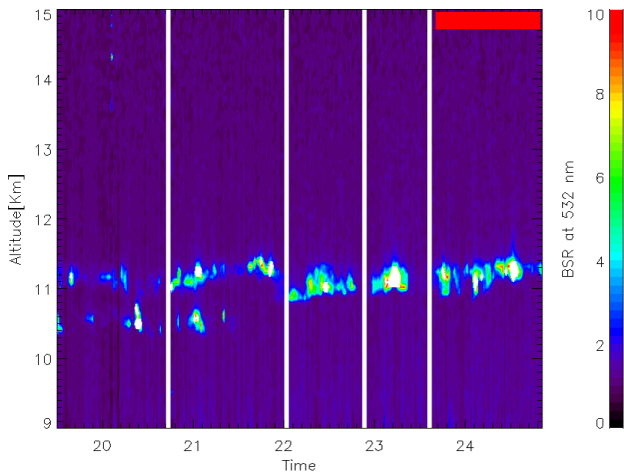


**Fig. 2b.** Contour plot of the backscattering ratio (BSR) calculated from the elastic channel at 532 nm for the lidar session at RTV between 19:31 and 00:50 UTC. White vertical lines identify the quasi-stationary periods. The horizontal red bar indicates the quasi-stationary period used in the Match approach (23:37–00:50 UTC).

### 4.3 Test case characterization

The temporal evolution of height, temperature and potential temperature ( $z$ ,  $T$  and  $\theta$ , respectively) between 11 March 2008 at 01:00 UTC and 14 March 2008 at 01:00 UTC for the cirrus envelopes, considered in Fig. 3, are shown in Fig. 4. Focusing on the trajectory parts at the very right-hand side of the graph, this figure reveals an essentially constant trend for  $\theta$  during the evolution between the two sites (air masses advected, roughly, along the same isentropic levels), except for the slight fluctuation of  $\approx 3/4$  K between the 15:00 UTC and 22:00 UTC on 13 March 2008 that, for the moment, will be neglected as well as the coincident fluctuation observed in the last part of  $z$  and  $T$  air mass evolution. On the contrary, a relevant constant increase (decrease) between 11 March 2008 at 04:00 UTC and 12 March 2008 at 04:00 UTC noticed when considering the  $z$  ( $T$ ) evolution of cirrus envelopes, will be discussed afterwards.

The previous analysis allows assuming a quasi-isentropic air mass transport between the two sites (between 13 March 2008 at 19:00 UTC and 14 March 2008 at 01:00 UTC, black horizontal bars in Fig. 4).

If we assume that the cirrus shape was evolving from both locations only due to crystal fall, the fulfilment of Match conditions permits one to use the difference between the two cirrus heights ( $\Delta z_{\text{cir}}$ ), measured by OHP and RTV lidars, corrected with the local isentropic shift ( $\Delta z_{\text{theta}}$ ), to estimate the mean crystal fall velocity ( $v_s$ ) between the two sites, following the simplified equation below:

$$v_s = (\Delta z_{\text{cir}} + \Delta z_{\text{theta}}) / \Delta t, \quad (1)$$

where  $\Delta t$  is the time spent by the air mass to go from one site to the other.

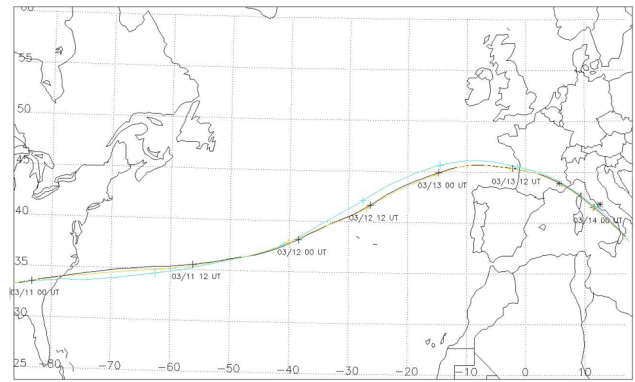


**Fig. 3.** Backward trajectories initialized 14 March 2008 at 01:00 UTC until 11 March 2008 at 01:00 UTC for three atmospheric levels (10.7, 11.2, 11.7 km; black, yellow and blue, respectively) that include bottom and top heights of the cirrus observed by OHP and RTV lidars. Stars points denote the positions of OHP (43.9° N/5.7° E) and RTV (41.8° N/12.7° E) sites, while plus points indicate the air mass temporal position every 12 h.

Equation (1) is valid only with the hypotheses of adiabatic transport and of “frozen” conditions inside the cirrus (i.e. cloud microphysical evolution and mesoscale fluctuations are not taken into account at this stage) between the two sites. We will assume these hypotheses in the remaining part of this section, while their validity will be discussed in the next section. For this “frozen” condition, the only mechanism of ice crystal destruction is by sedimentation, while any generating mechanisms of new ice crystals are not foreseen.

The first and the last quasi-stationary periods, respectively, at the OHP and RTV (see Table 3a and b), whose temporal distance corresponds to  $\Delta t$  (approximately 6 h), have been compared. The backscattering ratio profiles of the two cirrus clouds are reported in Fig. 5. The considered mid-cirrus height ( $z_{\text{cir}}$ ) are defined according to Chen et al. (2002):

$$z_{\text{cir}} = \frac{\int_{z_{\text{base}}}^{z_{\text{top}}} z' R(z') dz'}{\int_{z_{\text{base}}}^{z_{\text{top}}} R(z') dz'}, \quad (2)$$

namely the BSR mass centre of the cirrus (11.42 and 11.20 km, respectively for OHP and RTV periods, with  $dz_{\text{cir}} = 0.05$  km). Considering the height and isentropic shift (0.2 and approximately 0.1 km, respectively) between the two sites,  $v_f$  is approximately  $1.5 \text{ cm s}^{-1}$ .

Assuming that the terms of the sum in the right part of Eq. (1) are uncorrelated and if the uncertainty in  $\Delta t$  is neglected, the uncertainty ( $dv_s$ ) is mainly due to the separation contribution of the errors of these terms. In this study, only the uncertainty ( $d\Delta z_{\text{cir}}$ ) associated to  $\Delta z_{\text{cir}}$  has been considered, so that  $dv_s \approx d\Delta z_{\text{cir}}$ , derived by the propagation error formula, is approximately  $0.3 \text{ cm s}^{-1}$ .

**Table 3a.** Characterization of cirrus quasi-stationary periods identified at OHP through principal lidar parameters. Temperature values are derived from the operational radiosoundings launched from Nimes (80 km west from OHP).

UTC	18:48–19:20	21:38–22:50	22:53–23:41	23:43–01:46
Occurrence (min)	32	72	48	123
Geometric mean height (km)	11.42	11.40	11.30	11.30
Thickness (km)	0.5	1.0	1.0	0.8
Intensity of the mean BSR	$7.6 \pm 3.8$	$9.0 \pm 8.8$	$2.4 \pm 1.6$	$1.8 \pm 1.2$
Relative height (km)	0.19	0.17	0.07	0.07
Mean $T$ inside the cloud (K)	211	211	210	210
Optical depth (PI method, LR = 18.2 sr)	$0.026 \pm 0.001$	$0.051 \pm 0.001$	$0.024 \pm 0.001$	$0.009 \pm 0.001$
Optical depth (MI method)	$0.021 \pm 0.005$	$0.011 \pm 0.007$	$0.008 \pm 0.009$	$0.011 \pm 0.011$

**Table 3b.** Characterization of cirrus quasi-stationary periods identified at RTV through principal lidar parameters. Temperature values are derived from the operational radiosoundings launched from Pratica di Mare (25 km south-west from RTV).

UTC	19:31–20:43	20:44–21:51	21:52–23:06	23:07–23:36	23:37–00:50
Occurrence (min)	72	67	74	29	73
Geometric mean height (km)	10.75	10.90	11.10	11.10	11.20
Thickness (km)	1.07	1.3	0.7	0.6	0.7
Intensity of the mean BSR	$1.4 \pm 0.4$	$1.6 \pm 0.7$	$1.9 \pm 0.7$	$2.5 \pm 1.6$	$2.4 \pm 1.6$
Relative height (km)	−0.35	−0.20	0.00	0.00	0.05
Mean $T$ inside the cloud (K)	216	215	214	214	213
Optical depth (PI method, LR = 18.2 sr)	$0.003 \pm 0.001$	$0.007 \pm 0.001$	$0.005 \pm 0.001$	$0.008 \pm 0.001$	$0.011 \pm 0.001$
Optical depth (MI method)	$0.011 \pm 0.008$	$0.005 \pm 0.027$	$0.031 \pm 0.033$	$0.018 \pm 0.091$	$0.027 \pm 0.081$
Optical depth (Raman method)	$0.011 \pm 0.008$	$0.007 \pm 0.007$	$0.004 \pm 0.03$	–	$0.029 \pm 0.053$

Furthermore,  $v_s$  is also affected by the fact that larger crystals, during the advection between the two sites, could have disappeared and reformed before the cirrus was above the arrival site, with the result that the value of  $v_s$  could be underestimated. In the case considered, in fact, the height of  $z_{\text{cir}}$  for OHP cirrus was calculated including a part of the cirrus (the large peak at 11.4 km in Fig. 5) that is likely to be composed of large crystals. To roughly estimate this systematic error, it has been assumed that only survival small crystals, which are mostly present in the upper part of the OHP cirrus, cause the cirrus vertical displacement observed between OHP and RTV. With this assumption,  $z_{\text{cir}}$  at the OHP is equal to 11.51 km and the corresponding  $v_s$  is  $1.9 \text{ cm s}^{-1}$ .

Although, with single-wavelength measurements, it is not possible to distinguish which properties have evolved between two successive measurements, changes of the backscatter signal and in optical depth can most probably be associated with changes in the crystal size parameter during advection (Jumelet et al., 2008). In particular, from the lidar values of the quasi-stationary periods considered in Table 3a and b and the Fig. 5, the cirrus, in addition to lower in altitude, appears to extend its vertical thickness ( $\Delta z$  from 0.5 to 0.7 km) and simultaneously decrease its optical depth ( $\tau$  from 0.026 to 0.011, considering the values estimated with PI method) and the intensity of the mean BSC inside the cirrus (from 7.6 to 2.4). A similar variation in  $\tau$  is not highlighted

when comparing the values derived from the MI and Raman methods, but the great uncertainty affecting these values did not allow for making any further analysis. Using the values of  $\Delta z$  and  $\tau$  measured by the two lidar stations, it is possible to roughly evaluate the crystal mean radius variation. In fact, assuming a uniform mono-dispersed size distribution throughout the cloud depth and a constant extinction efficiency ( $Q_e$ ) of 2, the experimental ice crystal effective radius ( $r_{\text{exp}}$ ) for various number concentrations ( $N_0$ ) can be estimated, according to the following formula (Comstock et al., 2002):

$$r_{\text{exp}} = \sqrt{\frac{\tau}{N_0 \cdot \Delta z \cdot Q_e \cdot \tau}} \quad (3)$$

The comparison between the values of  $r_{\text{exp}}$  for the two considered periods highlights, for ice crystal population with the same number concentration, an effective radius reduction of more than 50 % that might be caused by the ice crystal sedimentation into sub-saturated air below the cirrus. In fact, on average, this process tends towards decreasing the population of large ice crystals (which fall out of the cloud layer and sublimate), favouring the persistence of small ice crystals.

Utilizing the range of values  $1.4\text{--}1.9 \text{ cm s}^{-1}$  for  $v_s$  and following the Stokes equation, it is possible, assuming spherical shape, to calculate the theoretical mean radius ( $r_{\text{th}}$ ) of crystals for the cirrus at the French departure site:

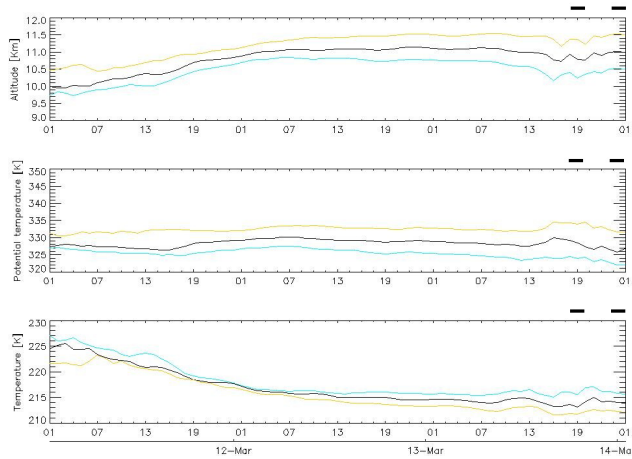


**Fig. 4.** Evolution of the altitude, potential temperature and temperature of the air mass backward trajectories between 11 March 2008 at 01:00 UTC and 14 March 2008 at 01:00 UTC for three atmospheric levels (10.7, 11.2, 11.7 km; black, yellow and blue, respectively) that include bottom and top heights for the cirrus observed by OHP and RTV lidars. Horizontal delimited black bars indicate air mass passage above OHP and RTV sites (13 March 2008 at around 19:00 UTC and 14 March 2008 at 01:00 UTC, respectively).

$$r_{\text{th}} = \sqrt{\frac{9}{2} \cdot \frac{v_s \mu}{(\rho_i - \rho_a) g}}, \quad (4)$$

where  $\mu$  is the dynamic viscosity of the air,  $\rho_i$  and  $\rho_a$  are, respectively, the mass density of ice and air, and  $g$  is the gravitational acceleration. For the values of temperature and pressure, derived from Nimes radiosounding,  $r_{\text{th}}$  is equal to 9.9–11.5  $\mu\text{m}$ . From the comparison of these values to the set of  $r_{\text{exp}}$  in Table 4, it is possible to deduce the corresponding values of  $N_0$  and then to estimate qualitatively the OHP cirrus ice water content (IWC), which is roughly 0.1–0.01  $\text{mg m}^{-3}$ .

The value of  $v_s$  (1.4–1.9  $\text{cm s}^{-1}$ ), estimated for the cirrus observed by OHP and RTV lidar systems during the night from 13 to 14 March 2008, is consistent with the types of crystals that are likely to compose a high altitude, optically thin, cold cirrus, namely crystals with simple shapes and small dimensions. Furthermore, the qualitative values of  $r$  and IWC derived for the cirrus ( $\approx 10 \mu\text{m}$  and 0.1–0.01  $\text{mg m}^{-3}$ , respectively) studied are comparable to those observed for SVCs in other studies (Immler et al., 2008, for northern mid-latitude SVC; Davis et al., 2010, for a tropical tropopause SVC).

Following mid-latitude cirrus classification derived from the lidar data of the French site (Keckhut et al., 2006), the case considered belongs to the thin tropopause class, which is characterized by low values of temperature, thickness and optical depth and a location in correspondence with the local tropopause. Several case studies (Keckhut et al., 2005; Montoux et al., 2010) relate the formation of this class to

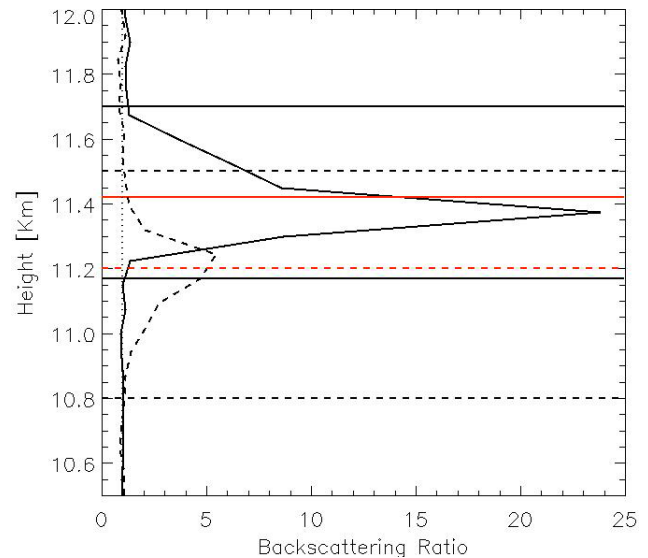


**Fig. 5.** Backscattering ratio profiles of the cirrus measured at OHP for the first quasi-stationary period (18:48–19:20 UTC, continuous line) and at RTV for the last quasi-stationary period (23:37–00:50, dashed line). Horizontal black lines identify the cirrus top and base heights, while the red lines indicate cirrus mid-heights.

large-scale transport processes (advection to mid-latitudes of clouds related to cumulonimbus clouds anvils or of moist tropical upper tropospheric air masses). This latter hypothesis (in particular the transport of moist air masses) could be the explanation for the formation of the considered cirrus. In fact, the drop in temperature by approximately 10 K experienced by the air mass during their transit over the western and central part of the Atlantic (see Fig. 4) corresponds to a slight air uplift of 1000 m in approximately 24 h ( $1.2 \text{ cm s}^{-1}$ ). This feature could be associated with an adiabatic process over the Atlantic Ocean bringing wet air to upper regions of the troposphere. The adiabatic cooling, associated with the observed air mass upward motion, could have resulted in an increase of ice saturation and favoured the formation and growth of ice crystals (Jensen et al., 1996; Boehm et al., 1999). Therefore, the considered cirrus seems to relate to the air transport of small-scale filamentary structures extending for a couple of hundred of kilometers horizontally and with a vertical thickness of a few kilometers (Keckhut et al., 2005). Furthermore, with the relatively small size of ice crystals (radius  $\approx 10 \mu\text{m}$ ), as in the case considered, cloud radiative heating could generate a circulation (with rising inside the cloud, sinking outside the cloud, entrainment at cloud base, detrainment at cloud top), which can provide a water supply for the cloud and substantially extend the cloud lifetime, as shown by Dinh et al. (2010).

**Table 4.** Estimates of effective ice crystal radius ( $r$ ) derived from Eq. (1) for the values of  $\Delta z$  and  $\tau$  of the cirrus quasi-stationary periods considered in the Match approach. Calculations are made for five different ice crystal number concentrations ( $N_0$ ).

$N_0$ [number $\text{cm}^{-3}$ ]	OHP $r$ [ $\mu\text{m}$ ]	RTV $r$ [ $\mu\text{m}$ ]
0.05	12.9	6.0
0.1	9.1	4.3
0.5	4.1	1.9
1	2.9	1.3
5	1.3	0.6

#### 4.4 Test case uncertainties and consistency

As stated in Sect. 3, one of the main requirements to provide meaningful Match observations is a correct value of  $R_{\text{max}}$ . In absence of any space-borne instrument information,  $R_{\text{max}} = 150$  km has been fixed on the basis of the structure characteristics of the observed cirrus (see Sect. 4.3) and  $R = 80$  km, resulting from Hysplit model, fulfilling this condition. However, at the RTV site the studied “quasi-stationary” time period is approximately 1 h long (from 23:37 to 00:50 UTC, see Fig. 2b), which, with a  $100 \text{ km h}^{-1}$  horizontal wind speed, could mean a “quasi-stationary” spatial extension of the cloud of 100 km. Thus, the fixed value of  $R_{\text{max}}$  appears to be too large and, for this case, a probably reliable value could be 50 km (centering the cloud on the air mass).

Another source of error, which has not been considered, is  $d\Delta z_{\text{theta}}$ , the uncertainty associated with air masses isentropic shift between the two sites. The representativeness of thermodynamic variables is a critical point in meteorological models and depends upon local effects as well as the larger scale gradients of the variable and how well a gridded field can represent a continuous function. The accurate estimation of this term is difficult and, for the aim of the paper, not necessary. However, if we consider that an error of 100 m would lead to  $d\Delta z_{\text{theta}} \approx 0.6 \text{ cm s}^{-1}$ , the vertical resolution of the Hysplit version used (50 hPa in upper troposphere) is not adequate for the required precision.

The analysis of backward trajectories is useful to discuss the validity of the “frozen” approach used in Sect. 4.3 to estimate  $v_s$  through Eq. (1). In particular, the Fig. 4 reveals that between 20:00–21:00 UTC on 13 March, in correspondence to the crossing of Maritime Alps, air masses seem to rise by 200 m, with an increase in temperature by 1 K. This behavior could be related to the effect of significant mixing processes of the air parcels exposed to orographic perturbations. In the case considered, the cirrus maintenance could have also been affected by the  $\Delta z_{\text{theta}} = 100$  m upward (and a corresponding cooling of 1 K) that could have caused to new ice nucleation. This could lead to a misinterpretation of cirrus shift that could be due to nucleation instead of sedimentation.

**Table 5.** Estimates of the principal error sources of the mean sedimentation velocity ( $v_s$ ) for the considered test case. Each uncertainty is tabulated in terms of quantified or qualitatively estimated relative error.

Source of error	quantified (relative error)	estimated (relative error)
$d\Delta z_{\text{cir}}$	20 %	–
$d\Delta z_{\text{micro}}$ (frozen conditions)	30 %	–
$d\Delta z_{\text{meso}}$	–	30 %
$d\Delta z_{\text{micro}}$	–	> 30 %
$d\Delta z_{\text{theta}}$	–	> 50 %

Furthermore, the advection over the Alps could trigger the formation of gravity waves. Several works have shown that mesoscale fluctuations induced by gravity waves in the upper troposphere and lower stratosphere considerably influence the formation and the evolution of high cirrus clouds (Haag and Kärcher, 2004; Jensen et al., 2005; Kärcher, 2012). The analysis of the observed lidar quasi stationary periods cannot provide information about these effects, excepting the consideration that the maximum mid-cirrus height displacement of the quasi stationary cirrus over the two sites is 100 m (from 11.4 to 11.3 km for OHP and from 11.1 to 11.2 km for three last quasi-stationary cirrus single layer periods for RTV; see Table 3a and b). This vertical displacement could be connected to the fact that temperature fluctuations on scales of hundred kilometres in the upper troposphere are of the order of 1 K (Gierens et al., 2007).

However, while accurate sedimentation values cannot be retrieved, the estimation of crystal fall velocities are useful whatever the processes involved.

The major uncertainty for retrieving the crystal fall velocity, as individual crystals cannot be observed, is the univocal link between the vertical cirrus shape given by the lidar backscatter ratio and the vertical distribution of the same crystals some time later. The vertical shape of the cirrus can also be due to multiple successive frozen/sublimation effects along the cirrus path or small-scale dynamical effects, such as those induced by gravity waves, that can modify the instantaneous temperature profile when lidar observation are performed. This uncertainty is mainly link to the fact that observations are performed at two given times and no information is available between both lidar observations.

From these considerations, it is clear that the terms regarding ice formation/sublimation and mesoscale fluctuations cannot be neglected in Eq. (1), in particular if the sites are relatively distant, as in the case of OHP and RTV. The a priori assumptions of “frozen” conditions and isentropic transport need to be verified to quantitatively apply this methodology to cirrus studies.

To overcome this difficulty (i.e. to verify the processes to which cirrus crystals are subjected during the transport from one site to the other), several improvements can be

proposed. The first one consists in increasing the observation sampling in using, for example, other lidar stations, reduced distances between stations and/or additional observations using space measurements, as can be provided by CALIOP (Cloud-Aerosol Lidar with Orthogonal Polarization), the space-borne lidar installed on CALIPSO (Cloud Aerosol Lidar and Infrared Pathfinder Satellite Observation). Another possible tool to track cirrus advection could be the use of satellite data from passive space-borne instruments. In our case, the small optical thickness of the cirrus limited the use of passive sensors (we do not have any geostationary images) while coincident CALIOP lidar-tracks were not available.

Another approach is to use numerical simulations with high resolution to reproduce the small-scale dynamics. An employment of cirrus microphysical-resolved models (such as Weather Research and Forecasting, WRF, Gu et al., 2011) is necessary to simulate and monitor the effect of these fluctuations on the evolution of cirrus properties between the two sites. For this purpose, collocated temperature measurements are also recommended in substitution of operational radiosoundings that, in the case of OHP, are 80 km away from the lidar station.

Finally, another improvement will consist in having a better description of micro-physic parameters to be able to understand if the vertical cirrus shape evolution is consistent with micro-physic changes. Lidars with additional wavelengths, polarizations, and Raman nitrogen references allow size-distribution and form descriptions.

Table 5 summarizes, for the considered test case, the principal error sources of the mean sedimentation velocity ( $v_s$ ), derived by the Match–lidar method, in terms of quantified or qualitatively estimated relative error.

## 5 Conclusions

In this work, an observation strategy to study the evolution of cirrus optical properties has been evaluated. This methodology, which couples lidar measurements through the Match approach, foresees characterization of mean significant changes in optical properties of cirrus quasi-stationary periods from the analysis of the lidar parameter variations observed between successive measurements located along the direction of the air mass advection. To assess its feasibility, the technique has been tested using the existing subsamples of datasets (2007–2008) of OHP and RTV lidars, which are located along one of the typical directions of the front progression in the Mediterranean area, and exhibiting similar instrumental characteristics in terms of emitted wavelengths, data resolution and performances. Applying to this dataset a common algorithm procedure and the proposed cirrus Match approach, a test case of upper tropospheric thin cirrus observed by the two instruments during the night from 13 to 14 March 2008 has been identified and studied. To estimate

the main uncertainties characterizing the adopted approach, assumptions on a quasi-isentropic air mass transport and cirrus “frozen conditions” during the advection between the two sites have been made. These hypotheses allowed for using the first and the last quasi-stationary periods, measured, respectively, above the OHP and the RTV, to estimate the crystal cloud mean sedimentation velocity ( $v_s$ ) between the two sites. The range of retrieved values for  $v_s$  (1.4–1.9 cm s<sup>-1</sup>) is consistent with crystals of simple shapes and small dimensions. The uncertainty associated with this value, considering only the error of the term representing the difference between the two cirrus heights, is around 20%. One of the critical points in this estimation, attested by a range bar of more than 30%, is that, during advection, larger crystals, because of ice sedimentation, could have disappeared before the cirrus was above the arrival site, causing an underestimation of  $v_s$ . This effect has to be considered when calculating the cirrus height at the departure site. Moreover additional non-negligible uncertainties could derive from the error of the isentropic shift predicted by Hysplit model ( $d\Delta z_{\text{theta}} \approx 0.6 \text{ cm s}^{-1}$  for an error of 100 m), while the qualitative analysis of RTV quasi-stationary cirrus period casts doubts, for the test-case, on the suitability of the  $R_{\text{max}}$  value.

The main critical point of the technique is that, to reliably estimate  $v_s$ , the validity of the adopted assumptions has to be verified. In fact, during the transport from one site to the other, cirrus crystals are subjected to modification of their optical and physical properties. Therefore, the developed cirrus observing strategy, in addition to the fulfilment of the Match conditions, is exploitable only with a careful evaluation of dynamical changes and microphysical processes inside the cirrus during advection. In particular, mesoscale fluctuations could have a strong impact on cirrus formation and evolution and must be evaluated.

For these reasons, the value of  $v_s$  derived for the test case, although consistent with ice crystals composing high tropopause cirrus as those observed over the two sites, is characterized by a high number of uncertainties that compromise its scientific relevance. However, the considered Match case allowed achieving the objective of this work: to assess the technique feasibility and to fix the procedures to solve the main critical issues identified.

In conclusion, the developed Match–lidar method seems to be a valid tool to study the mean evolution of cirrus that have a large horizontal extension (hundred of km), long cloud lifetime (tens of hours) and a relatively small horizontal variability. The high vertical spatial and temporal resolution of lidar measurements together with a Lagrangian approach assure a characterization of cirrus optical parameters, in particular for those cirrus clouds, as SVCs, that are hardly observable through space-borne passive instruments. However, several uncertainties affect the technique and significant requirements have to be adopted to appropriately apply the methodology and to quantitatively determine the associated uncertainties:

- lidar stations must be located along frequent directions of air mass displacements, at a maximum distance of 200–300 km that allows distinguishing changes in main cirrus optical properties and that, at the same time, assures a high probability of Match events and a cirrus persistence between the two sites;
- high temporal and spatial variability of cirrus is a critical issue of adopting lidar–Match coupling to cirrus observations. To reduce the uncertainties associated with this variability, mean lidar quantities through the identification of quasi-stationary temporal periods have to be employed;
- a procedure to fix suitable value of match-radius ( $R_{\max}$ ) has to be developed on the basis of the cirrus characteristics (spatial extension and variability);
- multi-wavelength lidar measurements are required to quantitatively characterize the differences of LPPs (e.g. geometrical and optical thickness, back-scattering profile distribution) observed between two sites;
- lidar data have to be integrated with ancillary measurements (in situ and space-borne) of cirrus crystal size distribution, water vapour and temperature to characterize the processes to which cirrus are subjected during the transport from one site to another;
- the assumption of isentropic transport and “frozen” conditions inside the cirrus must be verified by using a microphysical cirrus model (WRF) to monitor the impact of mesoscale fluctuations and the evolution of microphysical cirrus processes between the two sites. The cirrus persistence could also be verified by the employment of CALIOP data to track cirrus advection.

Dedicated campaigns, which will fulfil the requirements listed above, are planned to study, through this approach, the mean micro-physical changes of mid-latitude cirrus clouds during advectons.

*Acknowledgements.* The authors thank Gian Luigi Liberti for the helpful discussions and Federico Angelini for his support on backward trajectory statistical processing. The authors acknowledge the NOAA Air Resources Laboratory (ARL) for the provision of the HYPLIT transport and dispersion model. OHP lidar activities are supported both by INSU and CNES. This work was also supported by the bilateral French–Italian project STRACLIMA. The research leading to these results has received funding from the European Union Seventh Framework Programme (FP7/2007–2013) and University of Versailles and Saint Quentin en Yvelines (UVSQ) under grant agreement RBUCE-UP No. 246556.

Edited by: R. Schofield



The publication of this article is financed by CNRS-INSU.

## References

- Ansmann, A., Wandinger, U., Riebesell, M., Weitkamp, C., and Michaelis, W.: Independent measurement of extinction and backscatter profiles in cirrus clouds by using a combined Raman elastic-backscatter lidar, *Appl. Optics*, 31, 7113–7113, 1992.
- Boehm, M. T., Verlinde, J., and Ackerman, T. P.: On the maintenance of high tropical cirrus, *J. Geophys. Res.*, 104, 24423–24434, 1999.
- Cadet, B., Giraud, V., Haefelin, M., Keckhut, P., Rechou, A., and Baldy, S.: Improved retrievals of the optical properties of cirrus clouds by a combination of lidar methods, *Appl. Optics*, 44, 1726–1734, 2005.
- Chen, W. N., Chiang, C. W., and Nee, J. W.: Lidar Ratio and Depolarization Ratio for Cirrus Clouds, *Appl. Optics*, 41, 6470–6476, 2002.
- Chepfer, H., Bony, S., Winker, D. M., Chiriaco, M., Dufresne, J.-L., and Seze, G.: Use of CALIPSO lidar observations to evaluate the cloudiness simulated by a climate model, *Geophys. Res. Lett.*, 35, L15704, doi:10.1029/2008GL034207, 2008.
- Comstock, J. M., Ackerman, T. P., and Mace, G. G.: Ground-based lidar and radar remote sensing of tropical cirrus clouds at Nauru Island: Cloud statistics and radiative impacts, *J. Geophys. Res.*, 107, 4714, doi:10.1029/2002JD002203, 2002.
- Congeduti, F., Marengo, F., Baldetti, P., and Vincenti, E.: The multiple-mirror lidar “9-eyes”, *J. Opt. A-Pure Appl. Op.*, 1, 185–191, 1999.
- Davis, S., Hlavka, D., Jensen, E., Rosenlof, K., Yang, Q., Schmidt, S., Borrmann, S., Frey, W., Lawson, P., Voemel, H., and Bui, T. P.: In situ and lidar observations of tropopause subvisible cirrus clouds during TC4, *J. Geophys. Res.*, 115, D00J17, doi:10.1029/2009JD013093, 2010.
- Deng, M. and Mace, G.: Cirrus microphysical properties and air motion statistics using cloud radar Doppler moments. Part I: Algorithm description, *J. Appl. Meteor. Clim.*, 45, 1690–1709, 2006.
- Dinh, T. P., Durran, D. R., and Ackerman, T.: The maintenance of tropical tropopause layer cirrus, *J. Geophys. Res.*, 115, D02104, doi:10.1029/2009JD012735, 2010.
- Dionisi, D., Congeduti, F., Liberti, G. L., and Cardillo, F.: Calibration of a Multichannel Water Vapor Raman Lidar through Non-collocated Operational Soundings: Optimization and Characterization of Accuracy and Variability, *J. Atmos. Ocean. Tech.*, 27, 108–121, 2010.
- Donovan, D. P. and van Lammeren, A. C. A. P.: Cloud effective particle size and water content profile retrievals using combined lidar and radar observations. Part 1: Theory and simulations, *J. Geophys. Res.*, 106, 27425–27448, 2001.
- Draxler, R. R. and Rolph, G. D.: HYSPLIT (Hybrid Single-Particle Lagrangian Integrated Trajectory) Model, NOAA ARL

- READY, NOAA Air Resources Laboratory, Silver Spring, MD, available at: <http://ready.arl.noaa.gov/HYSPLIT.php> (last access: 20 July 2012), 2003.
- Dupont, J. C., Haeffelin, M., Morille, Y., Noël, V., Keckhut, P., Winker, D., Comstock, J., Chervet, P., and Roblin, A.: Macro-physical and optical properties of midlatitude cirrus clouds from four ground-based lidars and collocated CALIOP observations, *J. Geophys. Res.*, 115, D00H24, doi:10.1029/2009JD011943, 2010.
- Ferrare, R. A., Turner, D. D., Heilman Brasseur, L., Feltz, W. F., Dubovick, O., and Tooman, T. P.: Raman lidar measurements of the aerosol extinction-to-backscatter ratio over the Southern Great Plains, *J. Geophys. Res.*, 106, 20333–20347, 2001.
- Gierens, K., Kohlhepp, R., Dotzek, N., and Smit, H. G.: Instantaneous fluctuations of temperature and moisture in the upper troposphere and tropopause region. Part I: Probability densities and their variability, *Meteorol. Z.*, 16, 221–231, 2007.
- Goldfarb, L., Keckhut, P., Chanin, M. L., and Hauchecorne, A.: Cirrus climatological results from lidar measurements at OHP, *Geophys. Res. Lett.*, 28, 1687–1690, 2001.
- Grund, C. J., Banta, R. M., George, J. L., Howell, J. N., Post, M. J., Richter, R. A., and Weickmann, A. M.: High-resolution Doppler lidar for boundary layer and cloud research, *J. Atmos. Ocean. Tech.*, 18, 376–393, 2001.
- Gu, Y., Liou, K. N., Ou, S. C., and Fovell, R.: Cirrus clouds simulations using WRF with improved radiation parameterization and increased vertical resolution, *J. Geophys. Res.*, 116, D06119, doi:10.1029/2010JD014574, 2011.
- Haag, W. and Kärcher, B.: The impact of aerosols and gravity waves on cirrus clouds at midlatitudes, *J. Geophys. Res.*, 109, D12202, doi:10.1029/2004JD004579, 2004.
- Hoareau, C., Keckhut, P., Sarkissian, A., Baray, J. L., and Durry, G.: Methodology for water monitoring in the upper troposphere with Raman lidar at Haute-Provence Observatory, *J. Atmos. Ocean. Tech.*, 26, 2149–2160, 2009.
- Heymsfield, A. and Miloshevich, L.: Parameterizations for the cross-sectional area and extinction of cirrus and stratiform ice cloud particles, *J. Atmos. Sci.*, 60, 936–956, 2003.
- Immler, F., Treffeisen, R., Engelbart, D., Krüger, K., and Schrems, O.: Cirrus, contrails, and ice supersaturated regions in high pressure systems at northern mid latitudes, *Atmos. Chem. Phys.*, 8, 1689–1699, doi:10.5194/acp-8-1689-2008, 2008.
- Jakob, C.: Ice clouds in numerical weather prediction models, edited by: Lynch, D. K., Sassen, K., Starr, D. O’C., and Stephens, G., *Cirrus*, Oxford University Press, 327–345, 2002.
- Jensen, E., Toon, O., Selkirk, H., Spinhirne, J., and Schoeberl, M.: On the formation and persistence of subvisible cirrus clouds near the tropical tropopause, *J. Geophys. Res.*, 101, 21361–21375, 1996.
- Jensen, E. J., Smith, J. B., Pfister, L., Pittman, J. V., Weinstock, E. M., Sayres, D. S., Herman, R. L., Troy, R. F., Rosenlof, K., Thompson, T. L., Fridlind, A. M., Hudson, P. K., Cziczko, D. J., Heymsfield, A. J., Schmitt, C., and Wilson, J. C.: Ice supersaturations exceeding 100 % at the cold tropical tropopause: implications for cirrus formation and dehydration, *Atmos. Chem. Phys.*, 5, 851–862, doi:10.5194/acp-5-851-2005, 2005.
- Jumelet, J., Bekki, S., David, C., and Keckhut, P.: Statistical estimation of stratospheric particle size distribution by combining optical modelling and lidar scattering measurements, *Atmos. Chem. Phys.*, 8, 5435–5448, doi:10.5194/acp-8-5435-2008, 2008.
- Kärcher, B.: Supersaturation Fluctuations in Cirrus Clouds Driven by Colored Noise, *J. Atmos. Sci.*, 69, 435–443, 2012.
- Keckhut, P., Hauchecorne, A., Bekki, S., Colette, A., David, C., and Jumelet, J.: Indications of thin cirrus clouds in the stratosphere at mid-latitudes, *Atmos. Chem. Phys.*, 5, 3407–3414, doi:10.5194/acp-5-3407-2005, 2005.
- Keckhut, P., Borchi, F., Bekki, S., Hauchecorne, A., and SiLaouina, M.: Cirrus classification at mid-latitude from systematic lidar observations, *J. Appl. Meteor. Clim.*, 45, 249–258, 2006.
- Keckhut, P., Perrin, J. M., Thuillier, G., Hoareau, C., Porteneuve, J. P., and Montoux, N.: Subgrid-scale cirrus observed by lidar at mid-latitude: variability of the cloud optical depth, *J. Appl. Remote Sens.*, submitted, 2013.
- Khvorostyanov, V. I. and Sassen, K.: Microphysical processes in cirrus and their impact on radiation: a mesoscale modeling perspective, edited by: Lynch, D. K., Sassen, K., Starr, D. O’C., and Stephens, G., *Cirrus*, Oxford University Press, 397–432, 2002.
- Lanzante, J. R.: Resistant, Robust and non-parametric techniques for the analysis of climate data: theory and examples, including applications to historical radiosonde station data, *Int. J. Climatol.*, 16, 1197–1226, 1996.
- Lehmann, R., von der Gathen, P., Rex, M., and Streibel, M.: Statistical analysis of the precision of the Match method, *Atmos. Chem. Phys.*, 5, 2713–2727, doi:10.5194/acp-5-2713-2005, 2005.
- Luo, Z. and Rossow, W. B.: Characterizing Tropical Cirrus Life Cycle, Evolution, and Interaction with Upper-Tropospheric Water Vapor Using Lagrangian Trajectory Analysis of Satellite Observations, *J. Climate*, 17, 4541–4563, 2004.
- Montoux, N., Keckhut, P., Hauchecorne, A., Jumelet, J., Brogniez, H., and David, C.: Isentropic modeling of a cirrus cloud event observed in the midlatitude upper troposphere and lower stratosphere, *J. Geophys. Res.*, 115, D02202, doi:10.1029/2009JD011981, 2010.
- Orr, B. W. and Kropfli, R. A.: A Method for Estimating Particle Fall Velocities from Vertically Pointing Doppler Radar, *J. Atmos. Ocean. Tech.*, 16, 29–37, 1999.
- Platt, C. M. R. and Dilley, A. C.: Determination of the cirrus particle single-scattering phase function from lidar and solar radiometric data, *Appl. Optics*, 23, 380–386, 1984.
- Rex, M., von der Gathen, P., Harris, N. R. P., Lucic, D., Knudsen, B. M., Braathen, G. O., Reid, S. J., De Backer, H., Claude, H., Fabian, R., Fast, H., Gil, M., Kyrö, E., Mikkelsen, I. S., Rummukainen, M., Smit, H. G., Stähelin, J., Varotsos, C., and Zaitcev, I.: In situ measurements of stratospheric ozone depletion rates in the Arctic winter 1991/1992: A Lagrangian approach, *J. Geophys. Res.*, 103, 5843–5853, 1998.
- Rex, M., von der Gathen, P., Braathen, G. O., Harris, N. R. P., Reimer, E., Beck, A., Alfier, R., Krüger-carstensen, R., Chipperfield, M., De Backer, H., Balis, D., O’Connor, F., Dier, H., Dorokhov, V., Fast, H., Gamma, A., Gil, M., Kyrö, E., Litynska, I., Mikkelsen, I. S., Molineux, M., Murphy, G., Reid, S. J., Rummukainen, M., and Zerefos, C.: Chemical ozone loss in the Arctic winter 1994/95 as determined by the Match technique, *J. Atmos. Chem.*, 32, 35–59, 1999.
- Sanderson, B. M., Piani, C., and Ingram, W. J.: Towards constraining climate sensitivity by linear analysis of feedback patterns in thousands of perturbed-physics GCM simulations, *Clim. Dynam.*, 30, 175–190, doi:10.1007/s00382-007-0280-7, 2008.

- Sassen, K. and Campbell, J. R.: A midlatitude cirrus cloud climatology from the facility for atmospheric remote sensing. Part I: Macrophysical and synoptic properties, *J. Atmos. Sci.*, 58, 481–496, 2001.
- Sassen, K., Wang, Z., and Liu, D.: Global distribution of cirrus clouds from CloudSat/Cloud-Aerosol Lidar and Infrared Pathfinder Satellite Observations (CALIPSO) measurements, *J. Geophys. Res.*, 113, D00A12, doi:10.1029/2008JD009972, 2008.
- Sassen, K., Wang, Z., and Liu, D.: Cirrus clouds and deep convection in the tropics: Insights from CALIPSO and CloudSat, *J. Geophys. Res.*, 114, D00H06, doi:10.1029/2009JD011916, 2009.
- Schmitt, C. G. and Heymsfield, A. J.: The Size Distribution and Mass-Weighted Terminal Velocity of Low-Latitude Tropopause Cirrus Crystal Populations, *J. Atmos. Sci.*, 66, 2013–2028, 2009.
- Sherlock, V. J., Garnier, A., Hauchecorne, A., and Keckhut, P.: Implementation and validation of a Raman backscatter lidar measurement of mid and upper tropospheric water vapour, *Appl. Optics*, 38, 5838–5850, 1999.
- Spichtinger, P. and Gierens, K. M.: Modelling of cirrus clouds – Part 1b: Structuring cirrus clouds by dynamics, *Atmos. Chem. Phys.*, 9, 707–719, doi:10.5194/acp-9-707-2009, 2009.
- Stubenrauch, C., Rossow, W., Scott, N., and Chedin, A.: Clouds as seen by satellite sounders (3I) and imagers (ISCCP). Part III: Spatial heterogeneity and radiative effects, *J. Climate*, 12, 3419–3442, 1999.
- Taylor, J. R., Randel, W. J., and Jensen, E. J.: Cirrus cloud-temperature interactions in the tropical tropopause layer: a case study, *Atmos. Chem. Phys.*, 11, 10085–10095, doi:10.5194/acp-11-10085-2011, 2011.
- Tinel, C., Testud, J., Pelon, J., Hogan, R., Protat, A., Delanoë, J., and Bouniol, D.: The retrieval of ice cloud properties from cloud radar and lidar synergy, *J. Appl. Meteorol.*, 44, 860–875, 2005.
- Von der Gathen, P., Rex, M., Harris, N. R. P., Lucic, D., Knudsen, B. M., Braathen, G. O., De Backer, H., Fabian, R., Fast, H., Gil, M., Kyrö, E., Mikkelsen, I. S., Rummukainen, M., Stählerin, J., and Varotsos, C.: Observational evidence for chemical ozone depletion over the Arctic in winter 1991–92, *Nature*, 375, 131–134, 1995.